



1 Title

2 Bias correction of gauge-based gridded product to improve extreme precipitation analysis in the

3 Yarlung Tsangpo-Brahmaputra River Basin

4

5 Author names and affiliations

6 Xian Luo<sup>1,2</sup>, Xuemei Fan<sup>1</sup>, Yungang Li<sup>1,2</sup>, and Xuan Ji<sup>1,2</sup>

7 <sup>1</sup>Institute of International Rivers and Eco-security, Yunnan University, Kunming, China

8 <sup>2</sup>Yunnan Key Laboratory of International Rivers and Transboundary Eco-security, Kunming, China

9

10 Address

11 Institute of International Rivers and Eco-security, Yunnan University,

12 South Section, East Outer Ring Road, Chenggong District, Kunming, China

13

14 Email

15 Xian Luo: [luoxian@ynu.edu.cn](mailto:luoxian@ynu.edu.cn)

16 Xuemei Fan: [fanxuemei7@163.com](mailto:fanxuemei7@163.com)

17 Yungang Li: [ygli@ynu.edu.cn](mailto:ygli@ynu.edu.cn)

18 Xuan Ji: [jixuan@ynu.edu.cn](mailto:jixuan@ynu.edu.cn)

19

20 Contact Author: Xian Luo ([luoxian@ynu.edu.cn](mailto:luoxian@ynu.edu.cn))

21 Second Contact Author: Yungang Li ([ygli@ynu.edu.cn](mailto:ygli@ynu.edu.cn))

22



23 **Abstract.** Critical gaps in the amount, quality, consistency, availability, and spatial distribution of  
24 rainfall data limit extreme precipitation analysis, and the application of gridded precipitation data  
25 are challenging because of their considerable biases. This study corrected Asian Precipitation Highly  
26 Resolved Observational Data Integration Towards Evaluation of Water Resources (APHRODITE)  
27 in the Yarlung Tsangpo-Brahmaputra River Basin (YBRB) using two linear and two nonlinear  
28 methods, and assessed their influence on extreme precipitation indices. The results showed that the  
29 original APHRODITE data tended to underestimate precipitation during the summer monsoon  
30 season, especially in the topographically complex Himalayan belt. Bias correction using  
31 complementary rainfall observations to add spatial coverage in data-sparse regions greatly improved  
32 the performance of extreme precipitation analysis. Although all methods could correct mean  
33 precipitation, their ability to correct the wet-day frequency and coefficient of variation were  
34 substantially different, leading to considerable differences in extreme precipitation indices.  
35 Generally, higher-skill bias-corrected APHRODITE data are expected to perform better than those  
36 corrected by lower-skill approaches. This study would provide reference for using gridded  
37 precipitation data in extreme precipitation analysis and selecting bias-corrected method for rainfall  
38 products in data-sparse regions.

39

## 40 **1 Introduction**

41 Extreme precipitation often leads to floods, debris flows, and other secondary disasters (Wang  
42 et al., 2017), and changes in the frequency and intensity of extreme precipitation profoundly  
43 influence both natural environment and human society profoundly (Easterling et al., 2000; Yucel  
44 and Onen, 2014). Rainfall observations provide a primary foundation for comprehending their long-



45 term variability and change in extreme precipitation (Alexander, 2016). Accurate rainfall data are  
46 necessary for flood protection and water resource management. However, due to scarce spatial  
47 coverage of rainfall stations, short-length rainfall records, and high proportions of missing data,  
48 observations currently available in some remote basins are clearly inadequate to capture their  
49 precipitation characteristics. In addition, observed rainfall data are usually difficult to collect in  
50 international river basins because many countries may not share or freely distribute data (Lakshmi  
51 et al., 2018).

52 The Yarlung Tsangpo-Brahmaputra River is the fourth largest river in the world in terms of  
53 flow (Kamal-Heikman et al., 2007), which is influenced profoundly by complex atmospheric  
54 dynamics and regional climate processes (Immerzeel et al., 2010; Pervez and Henebry, 2015).  
55 Because its agriculture and economy rely heavily on monsoon precipitation, the basin is particularly  
56 vulnerable to changing climate (Singh et al., 2016; Liu et al., 2018; Janes et al., 2019; Xu et al.,  
57 2019; Zhang et al., 2019). During the four summer monsoon months of June, July, August, and  
58 September (JJAS), extreme precipitation with large uncertainties leads to numerous floods (Kamal-  
59 Heikman et al., 2007; Dimri et al., 2016; Malik et al., 2016). However, the understanding on extreme  
60 precipitation in the Yarlung Tsangpo-Brahmaputra River Basin (YBRB) have a number of gaps  
61 because of its complex topographic interactions with atmospheric flows, lack of observations, and  
62 data sharing issues, which hinder effective flood management (Ray et al., 2015; Prakash et al., 2019).

63 Currently, different gridded rainfall products provide effective information over regional to  
64 global scales, which could be broadly classified into four categories: (1) gauge-based data sets that  
65 build on observations from rainfall stations; (2) products from numerical weather predictions or  
66 atmospheric models; (3) satellite-only products; and (4) combined satellite-gauge products. The



67 performance of these products varies from region to region (Duan et al., 2016). Given the  
68 heterogeneity of orography and climate in the YBRB, observing and modeling its precipitation are  
69 very challenging (Khandu et al., 2017). In addition, satellite products are less reliable because high  
70 convective rainfall generally takes place in the southern foothills of the Himalayas (Prakash et al.,  
71 2015). Compared with some other gauge-based products, the Asian Precipitation Highly Resolved  
72 Observational Data Integration Towards Evaluation of Water Resources (APHRODITE) dataset  
73 collected more rainfall observations across South Asia (Rana et al., 2015), which have been proved  
74 could better estimate spatial precipitation (Andermann et al., 2011). Nonetheless, the lack and  
75 uneven distribution of rainfall stations at high altitudes in the Tibetan Plateau and Himalayas may  
76 introduce uncertainty and affect the accuracy of APHRODITE (Rana et al., 2015; Chaudhary et al.,  
77 2017).

78 Numerous rainfall observations can be obtained from public databases, although their short  
79 record and static character limit their direct application in precipitation analysis (Donat et al., 2013).  
80 However, these data could be useful for bias correction of gauge-based gridded products by  
81 providing additional observations from the denser network of rainfall stations. On the other hand,  
82 ranging from simple linear scaling to more sophisticated nonlinear approaches, several methods  
83 have been developed to adjust global climate model (GCM) data (Teutschbein and Seibert, 2012).  
84 Similarly, these bias correction methods could be applied to correct gridded rainfall products in  
85 sparsely-gauged mountainous basins (He et al., 2017). It is important to study whether extreme  
86 precipitation analysis could be improved by bias correction of gridded precipitation data and how  
87 different methods would influence extreme precipitation indices.

88 This study evaluated different bias correction approaches for APHRODITE in the YBRB and



89 assessed their effects on extreme precipitation analysis. We first corrected APHRODITE dataset by  
90 both linear and nonlinear methods, and then evaluated their performances. Next, we calculated  
91 extreme precipitation indices using the original and different corrected APHRODITE to further  
92 investigate the effects of bias correction on extreme precipitation analysis. The results would support  
93 reference for the application of gridded precipitation data and bias-corrected methods in extreme  
94 precipitation analysis.

95

## 96 **2 Material and methods**

### 97 **2.1 Study area**

98 The YBRB can be divided into three physiographic zones: (1) the Tibetan plateau (TP),  
99 covering 44.4% of the basin, with elevations above 3500 m; (2) the Himalayan belt (HB), accounting  
100 for 28.6% of the basin, with elevations ranging from 100 m to 3500 m; and (3) the floodplains (FP),  
101 covering 27.0% of the basin, with elevations up to 100 m (Immerzeel, 2008).

102 The moisture in the YBRB is mainly from the Indian Ocean. The YBRB exhibits a broad range  
103 of precipitation from the semi-arid upstream areas to the HB characterized by abundant orographic  
104 rainfall as well as the vast humid FP. In the upstream areas, precipitation is concentrated during  
105 JJAS, and rainfall intensity is mostly low due to long-distance moisture transport (Guan et al., 1984).  
106 The irregular topographic variations in the Himalayas profoundly affect the spatial distribution of  
107 precipitation by altering monsoonal flow, producing intense orographic rainfall along the Himalayan  
108 foothills (Khandu et al., 2017). The downstream areas also receive high rainfall from monsoon flow  
109 during JJAS, accounting for 60%–70% of the annual rainfall (Gain et al., 2011).

110



111 **2.2 Data sources**

112 **2.2.1 Observational data**

113 In the upper YBRB, rainfall data across China recorded at 31 meteorological stations were  
114 collected from the National Meteorological Information Center (NMIC, sourced from the China  
115 Meteorological Data Sharing Service System). In addition, data observed at 91 rainfall stations in  
116 the downstream area were obtained from the Global Historical Climatology Network  
117 (GHCN)–Daily for bias correction. GHCN–Daily comprises observations from four sources, which  
118 have been undergone extensive quality reviews, including the U.S. Collection, the International  
119 Collection, the Government Exchange Data, and the Global Summary of the Day. The locations of  
120 rainfall stations are shown in Fig. 1.

121

122 **2.2.2 APHRODITE**

123 Numerous rainfall observations were incorporated into APHRODITE, including (1) Global  
124 Telecommunication System (GTS)-based data, (2) data obtained from other projects or  
125 organizations, and (3) their own collection. The ratios of rainfall observations after quality control  
126 to the world climatology were calculated and interpolated for each month. The interpolated ratios  
127 were multiplied by the world climatology, and the first six components of the fast Fourier transform  
128 of the resulting values were used to obtain daily precipitation (Yatagai et al., 2012).

129 Daily rainfall data of APHRO\_MA\_025deg\_V1101 ([http://aphrodite.st.hirosaki-](http://aphrodite.st.hirosaki-u.ac.jp/index.html)  
130 [u.ac.jp/index.html](http://aphrodite.st.hirosaki-u.ac.jp/index.html)) at 0.25° resolution in the Asian monsoon area end in 2007, while recently  
131 published APHRO\_MA\_025deg\_V1101EX\_R1 (<http://aphrodite.st.hirosaki-u.ac.jp/index.html>),  
132 using the same algorithm and spatial resolution, extend the time series over the period 2007–2015.



133 Therefore, extreme precipitation could be analyzed during 1951–2015 by applying both datasets.  
134 To investigate the influence of topography on bias-corrected APHRODITE, the APHRODITE grids  
135 were classified into three topographic zones (the TP, HB, and FP; Fig. 2).

136

## 137 2.3 Methods

### 138 2.3.1 Bias correction methods

139 Two linear methods (linear scaling (LS) and local intensity scaling (LOCI)) and two non-linear  
140 methods (power transformation (PT) and quantile–quantile mapping (QM)) were used for bias  
141 correction in this study.

142 (1) LS

143 LS corrects monthly estimates in accordance with observations (Lenderink et al., 2007). It  
144 adjusts APHRODITE using the ratio between mean monthly observations and corresponding  
145 estimations:

$$146 \quad P_{APH}^*(d) = P_{APH}(d) \cdot \left[ \frac{\mu_m(P_{obs}(d))}{\mu_m(P_{APH}(d))} \right] \quad (1)$$

147 where  $P_{APH}(d)$  and  $P_{APH}^*(d)$  are the original and corrected APHRODITE, respectively.  
148  $\mu_m(P_{obs}(d))$  and  $\mu_m(P_{APH}(d))$  are the mean monthly observation and corresponding  
149 APHRODITE, respectively.

150 (2) LOCI

151 LOCI makes a flexible adjustment to the wet-day frequency and intensity (Schmidli et al., 2006;  
152 Teutschbein and Seibert, 2012). Firstly, an adjusted precipitation threshold ( $P_{th,APH}$ ) is determined  
153 so that the threshold exceedance matches the wet-day frequency of the observation. Secondly, a  
154 linear scaling factor for wet days is computed, using the mean monthly precipitation:



$$s = \frac{\mu_m(P_{obs}(d)|P_{obs}(d) > 0 \text{ mm})}{\mu_m(P_{APH}(d)|P_{APH}(d) > P_{th,APH}) - P_{th,APH}} \quad (2)$$

156 Finally, the precipitation data are corrected, using:

$$P_{APH}^*(d) = \max(s \cdot (P_{APH}(d) - P_{th,APH}), 0) \quad (3)$$

158 (3) PT

159 PT corrects both the mean and the coefficient of variation of precipitation (Leander and  
160 Buishand, 2007), changing precipitation by:

$$P_{APH}^*(d) = a \cdot (P_{APH}(d))^b \quad (4)$$

162 where  $a$  and  $b$  are the parameters of the power transformation, which are obtained using a  
163 distribution-free approach and estimated for each month within a 90-day window. Using a root-  
164 finding algorithm, the value of  $b$  is firstly determined to ensure that the coefficient of variation of  
165 the corrected precipitation matches that of the observed precipitation. The parameter  $a$  is then  
166 calculated using the mean observation and the corresponding mean of the transformed values.

167 (4) QM

168 By shifting occurrence distributions, QM corrects the distribution function of the APHRODITE  
169 to match those of the observed distribution function. A Gamma distribution is usually assumed for  
170 precipitation events and has been proven to be effective in precipitation analysis (Teutschbein and  
171 Seibert, 2012):

$$f_\gamma(x|\alpha, \beta) = x^{\alpha-1} \cdot \frac{1}{\beta^\alpha \cdot \Gamma(\alpha)} \cdot e^{-\frac{x}{\beta}}; x \geq 0; \alpha, \beta > 0 \quad (5)$$

173 where  $\alpha$  and  $\beta$  are the shape parameter and scale parameter, respectively.

174 The cumulative density function (CDF) for the APHRODITE is matched with that for the daily  
175 observed precipitation for a given month, and the daily precipitation for APHRODITE is corrected  
176 depending on its quantile. It should be noted that for APHRODITE, many days had low precipitation





177 estimates instead of substantial dry conditions, which may distort the distribution of daily  
178 precipitation. Therefore, an adjusted precipitation threshold is also used to ensure the wet-day  
179 frequency of the corrected APHRODITE match the observed frequency:

$$180 \quad P_{APH}^*(d) = \begin{cases} 0, & \text{if } P_{APH}(d) < P_{th,APH} \\ F_{\gamma}^{-1}\left(F_{\gamma}\left(P_{APH}(d)\right)\left|\alpha_{APH,m}, \beta_{APH,m}\right.\right)\left|\alpha_{obs,m}, \beta_{obs,m}\right., & \text{otherwise} \end{cases} \quad (6)$$

181  $F_{\gamma}$  and  $F_{\gamma}^{-1}$  are the Gamma CDF and its inverse, respectively.

182 Hereafter, the APHRODITE data corrected by LS, LOCI, PT, and QM are referred as LS-  
183 APHRODITE, LOCI-APHRODITE, PT-APHRODITE, and QM-APHRODITE, respectively.

184

### 185 2.3.2 Evaluation of APHRODITE estimates

186 Observed data from rainfall stations were applied to evaluate the performances of the original  
187 and corrected APHRODITE at daily scale. Five common statistical metrics, including Pearson  
188 correlation coefficient ( $r$ ), percentage bias ( $PB$ ), mean error ( $ME$ ), mean absolute error ( $MAE$ ), and  
189 root mean squared error ( $RMSE$ ), were calculated (Duan et al., 2016), and their equations and  
190 optimal values are summarized in Table 1.

191

### 192 2.3.3 Indices of extreme precipitation

193 To characterize extreme precipitation during JJAS, six indices recommended by the Expert  
194 Team on Climate Change Detection and Indices (ETCCDI), including consecutive wet days (CWD),  
195 number of heavy precipitation days (R10mm), number of very heavy precipitation days (R20mm),  
196 maximum 1-day precipitation amount (Rx1d), maximum 5-day precipitation amount (Rx5d), and  
197 simple daily intensity index (SDII), were applied in this study. Detailed descriptions of these indices  
198 are shown in Table 2. The indices fall roughly into three categories: (1) duration indices, which



199 represent the length of the wet spell; (2) threshold indices, which count the days on which a fixed  
200 precipitation threshold is exceeded; (3) absolute indices, which describe the maximum 1-day or 5-  
201 day precipitation amount (Sillmann et al., 2013).

202 In the grids distributed with rainfall stations, these six indices were calculated from the  
203 corrected APHRODITE. In addition, spatial interpolation was performed using inverse distance  
204 weighted (IDW) to obtain extreme precipitation indices for other grids within the basin. This  
205 allowed us to calculate mean values for each of the three topographic zones.

206

### 207 3 Results

#### 208 3.1 Evaluation of original and corrected APHRODITE estimates

209 The statistical metrics for daily precipitation during JJAS calculated for both original and  
210 corrected APHRODITE are summarized in Table 3. In general, original APHRODITE estimated  
211 precipitation well during JJAS in the YBRB, yielding  $r$  close to 0.8 in all three zones. However, the  
212  $PB$  of the original APHRODITE estimates in the TP, HB, and FP were  $-9.4$ ,  $-24.2$ , and  $-11.4$ ,  
213 respectively. This indicates that they tended to underestimate precipitation. Due to the high  
214 orographic precipitation coupled with the low density of rainfall stations used in the APHRODITE,  
215 underestimation in the HB with complex topography was greatest.

216 Corrected APHRODITE estimates yielded better statistical metrics. The  $PB$  and  $ME$  for LS-,  
217 LOCI-, and PT-APHRODITE were almost 0, indicating there was no longer any distinct bias in the  
218 mean of daily precipitation. The linear approaches and PT calculate correction values based on the  
219 ratio between long-term observations and APHRODITE estimates. Therefore, LS-, LOCI-, and PT-  
220 APHRODITE agreed with the mean observations. In the case of QM-APHRODITE, the  $PB$  in the



221 TP, HB, and FB were 3.2, 11.3, and 5.7, respectively, which were larger than those for other  
222 corrected APHRODITE estimates.

223 The other three statistical metrics ( $r$ ,  $MAE$ , and  $RMSE$ ) for the corrected APHRODITE in the  
224 TP were similar to those for the original APHRODITE, while the corrected APHRODITE in the FP  
225 had slightly higher  $r$  and lower  $MAE$  and  $RMSE$ . In the HB, the  $r$ ,  $MAE$ , and  $RMSE$  for the original  
226 APHRODITE were 0.81, 3.6 mm, and 15.9 mm, respectively; while for the corrected APHRODITE,  
227 the  $r$  were all higher than 0.9, and the  $MAE$  and  $RMSE$  were mostly less than 3 mm and 10 mm,  
228 respectively, suggesting that the greatest improvement occurred in the HB.

229

### 230 **3.2 The influence of bias correction on extreme precipitation indices**

#### 231 **3.2.1 Spatial distribution of extreme precipitation**

232 Rainstorms over the lower YBRB usually have a duration of 2–3 days (Dhar and Nandargi,  
233 2000), and large multi-day precipitation events are crucial to the floods in the basin. Hence, the  
234 spatial distribution of Rx5d during JJAS based on the original APHRODITE estimates were  
235 compared with the corrected APHRODITE estimates in Fig. 3. For the original APHRODITE, the  
236 area with Rx5d higher than 300 mm only accounted for 2.0% of the basin, while the proportions for  
237 LS-, LOCI-, PT-, and QM-APHRODITE were 10.9%, 18.7%, 21.7%, and 21.3%, respectively. The  
238 most profound difference between the original and corrected APHRODITE occurred over the  
239 windward slopes of the Himalayas before the river flows into the Brahmaputra valley. The Rx5d  
240 calculated from the original APHRODITE were lower than 300 mm, while much higher Rx5d were  
241 obtained after bias correction, yielding maxima of 946.6, 1030.3, 1105.1, and 1396.6 mm for LS-,  
242 LOCI-, PT-, and QM-APHRODITE, respectively. The eastern Himalayas, acting as orographic



243 barriers, push the southwest moist air upwards, leading to heavier extreme precipitation over the  
244 windward slopes (Singh et al., 2004; Bookhagen and Burbank, 2010; Dimri et al., 2016). However,  
245 original APHRODITE estimates tended to substantially underestimate these extreme precipitation,  
246 likely because of sparse rainfall gauge data. Besides aforementioned region, higher Rx5d along the  
247 Himalayan front were also found after bias correction. In this case, extreme precipitation calculated  
248 from nonlinear approaches were heavier than those derived from linear methods. Bias correction are  
249 able to consider topographic effects on the spatial distribution of extreme precipitation more  
250 comprehensively by making use of observations from denser network of rainfall stations. This  
251 resulted in better capturing of the main climatological features of extreme precipitation in the YBRB.

252

### 253 **3.2.2 Extreme precipitation indices in the three physiographic zones**

254 Sparsely distributed rainfall stations and short records affect the accuracy of spatial  
255 precipitation interpolation. Hence, it is hard to directly evaluate extreme precipitation obtained from  
256 bias-corrected APHRODITE by carrying out pixel-to-pixel comparison with those interpolated  
257 using gauge observations. A major limitation is the remaining uncertainty regarding how well  
258 different corrected APHRODITE estimate heavy rainfall, especially in data-sparse regions. Despite  
259 improved statistical metrics for bias-corrected APHRODITE, these could not guarantee good  
260 performance in extreme precipitation analysis. To obtain valuable information about the influences  
261 of bias-corrected methods on extreme precipitation analysis, extreme precipitation indices  
262 calculated from the original and four corrected APHRODITE were compared.

263 Extreme precipitation indices calculated from the original and four corrected APHRODITE  
264 estimates in the three different physiographic zones are shown in Fig. 4. The CWD estimated using



265 original APHRODITE and LS-APHRODITE were similar. Meanwhile, those derived from LOCI-,  
266 PT-, and QM-APHRODITE estimates were much less. For the original APHRODITE, there were a  
267 lot of days with low precipitation estimations instead of substantial dry conditions, leading to the  
268 overestimation on CWD. Likewise, this propagated to the LS-APHRODITE, because there was no  
269 change made to the wet-day frequency. In contrast, for both LOCI- and QM-APHRODITE, these  
270 low precipitation days were redefined as dry days using precipitation threshold, resulting in more  
271 reliable CWD. Finally, although the PT did not correct wet-day frequency, the CWD for the PT-  
272 APHRODITE were lower because tiny precipitation were also corrected.

273 Mean R10mm during JJAS obtained by the original APHRODITE estimates in the TP, HB, and  
274 FP were 6.7, 31.0, and 47.7 days, respectively. These were similar to those estimated by the bias-  
275 corrected APHRODITE datasets. However, the differences in R20mm were much pronounced.  
276 Mean R20mm in HB and FP for the bias-corrected APHRODITE datasets were close to 19.0 and  
277 26.5 days, respectively, which were approximately 4–5 days higher than those derived from the  
278 original APHRODITE estimates.

279 Compared with the original APHRODITE estimates, the Rx1d and Rx5d increased greatly after  
280 bias correction. In the HB, the mean Rx1d obtained from the original APHRODITE estimates was  
281 49.5 mm, while those for LS-, LOCI-, PT-, and QM-APHRODITE estimates were 72.4, 90.1, 109.0,  
282 and 103.8 mm, respectively. In addition, the range of Rx1d and Rx5d also increased considerably.  
283 LS was not able to adjust the coefficient of variation, resulting in the lowest Rx1d and Rx5d among  
284 the corrected estimates. Likewise, although precipitation intensity was changed, the Rx1d and Rx5d  
285 for the LOCI-APHRODITE were not as high as those obtained from the two nonlinear corrections,  
286 because it used consistent ratio in its linear transformation.



287 The differences in SDII between the original and corrected APHRODITE estimates were also  
288 marked. For example, the mean SDII in the FP calculated from the original APHRODITE estimates  
289 was 13.4 mm. After correction, the mean SDII for LOCI- and QM-APHRODITE estimates  
290 increased to 23.4 and 25.1 mm, respectively. These values were much greater than those derived  
291 from LS- and PT-APHRODITE datasets (15.7 and 17.7 mm). The original APHRODITE estimates  
292 are expected to underestimate SDII. Firstly, the original APHRODITE tended to underestimate  
293 precipitation, resulting in very high precipitation in the HB and TP not being fully captured.  
294 Secondly, the original APHRODITE overestimated wet days instead of substantial dry conditions,  
295 which distorted the estimation of precipitation intensity. Larger values of SDII obtained from the  
296 corrected APHRODITE estimates were expected, and the SDII for LOCI- and QM-APHRODITE  
297 were higher because they correct rainfall amount as well as number of rainy days.

298

### 299 **3.2.3 Relative changes in extreme precipitation indices**

300 The relative changes in extreme precipitation indices during JJAS based on the original and  
301 corrected APHRODITE estimates are shown in Fig. 5. The CWD for LOCI-, PT-, and QM-  
302 APHRODITE were all lower than the original APHRODITE, yielding relative change rates from  
303  $-66\%$  to  $-27\%$ . This indicates bias corrections decreased the number of rainy days except LS. The  
304 variations in R10mm and R20mm illustrated that the corrected APHRODITE identified much more  
305 extreme precipitation events in the TP. The changes in indices varied considerably for different  
306 correction methods, with the change rates of R20mm in the TP for LS-, LOCI-, PT-, and QM-  
307 APHRODITE being 30.4%, 169.2%, 297.1%, and 317.4%, respectively. For Rx1d, Rx5d, and SDII,  
308 the increases in the HB were much pronounced than those in the FP and TP. Except for the LS-



309 APHRODITE, the increases in Rx1d and Rx5d in the HB were all above 70% for the corrected  
310 APHRODITE estimates. Clearly, topographic variations profoundly influenced the spatial  
311 distribution of precipitation by altering monsoonal flow, resulting in considerable orographic rainfall  
312 on the windward slopes of the Himalayas (Khandu et al., 2017). Insufficient gauge observations in  
313 the Himalayas caused high uncertainty in the heavy precipitation estimates for the original  
314 APHRODITE. After bias adjustment especially those of nonlinear correction, the heterogeneous  
315 orographic effects on extreme precipitation were captured more accurately.

316

#### 317 **3.2.4 Interannual variation of extreme precipitation**

318 To investigate the interannual variation of extreme precipitation for the original and corrected  
319 APHRODITE, the exceedance probabilities of area-averaged Rx5d during JJAS were compared  
320 (Fig. 6). The Rx5d for corrected APHRODITE differ considerably, and the LOCI-, PT-, and QM-  
321 APHRODITE estimated much higher Rx5d than the original APHRODITE and LS-APHRODITE.  
322 In addition, there were greater variability in the Rx5d derived from PT- and QM-APHRODITE. In  
323 particular, heavier Rx5d with low exceedance probabilities obtained by nonlinear corrections  
324 reflected the increasing interannual variation.

325

#### 326 **4 Discussion**

327 Using two linear and two bias nonlinear methods, we corrected APHRODITE estimates during  
328 JJAS in the YBRB to investigate the effects of different approaches on extreme precipitation  
329 analysis. Regardless of the method used, bias correction improved the performance of rainfall  
330 estimates. Nonetheless, extreme precipitation indices were strongly dependent on the bias correction



331 approach applied.

332 A primary problem when using gauge-based gridded data sets for extreme precipitation  
333 analysis is the fundamental mismatch between point-based observations and gridded estimates  
334 (Alexander, 2016). In addition, the spatial coverage of rainfall stations is another major source of  
335 uncertainty, particularly where spatial distributions of precipitation are complex (Donat et al., 2013).  
336 There are currently several approaches for bias correction, ranging from simple linear scaling to  
337 more sophisticated nonlinear methods (Teutschbein and Seibert, 2012). Although mean precipitation  
338 corrected by all bias-corrected approaches were similar, their standard deviations and consequent  
339 extreme precipitation indices varied considerably. In the case of linear corrections, both mean and  
340 standard deviation are multiplied by same factor (Leander and Buishand, 2007), resulting in dubious  
341 variations of precipitation. Nonlinear corrections adjust mean and also coefficient of variation  
342 (Teutschbein and Seibert, 2012), yielding more reliable results. In addition, the typical biases of  
343 rainfall products are related to their identification of too many wet days with low-intensity  
344 precipitation. Among the four bias-corrected approaches applied herein, LS and PT make no change  
345 on the number of rainy days, while LOCI and QM use threshold exceedance to match the wet-day  
346 frequency to the observations. Overall, QM corrects most of the statistical characteristics, and  
347 therefore it is expected to perform better in extreme precipitation analysis.

348 In international river basins, rainfall data are usually not publicly available, and extreme  
349 precipitation analysis may suffer from data restrictions (Nishat and Rahman, 2009; Luo et al., 2019).  
350 Several great international rivers in south Asia, including the Indus, Ganges, and Yarlung  
351 Tsangpo–Brahmaputra, originate from or flow through the Himalayas. Rainfall estimates of  
352 different products varied markedly along the Himalayan front and obtained similar results toward





353 the adjacent low-relief domains (Andermann et al., 2011). The GHCN-Daily data can be applied to  
354 adjust gauge-based gridded data sets in this region, ensuring these products capture the spatial  
355 distribution and variation of extreme precipitation. However, numerous GHCN-Daily records in  
356 Asia do not contain data from recent years, and the short or incomplete rainfall records limit their  
357 direct applications (Donat et al., 2013). Hence, it would be preferable to add spatial coverage in  
358 data-sparse regions by applying nonpublic datasets.

359

## 360 **5 Conclusions**

361 Despite increasing use of gridded rainfall products in sparsely gauged river basins, their  
362 application in extreme precipitation analysis is challenging due to considerable biases. This study  
363 made use of four methods to correct the APHRODITE in the YBRB. Their influences on extreme  
364 precipitation indices were compared and assessed. The following conclusions were drawn.

365 (1) Original APHRODITE tended to underestimate precipitation during JJAS, and bias  
366 correction improved the accuracy of APHRODITE, especially in the HB with complex topography,  
367 highlighting the superiority of corrected APHRODITE.

368 (2) The extreme precipitation indices calculated from different corrected APHRODITE varied  
369 substantially, depending on correction method and location. Major dissimilarities were induced by  
370 wet-day frequency and standard deviation. Nonlinear correction methods adjust not only mean  
371 precipitation but also coefficient of variation, and QM further corrects probability of wet days,  
372 which is expected to perform better in extreme precipitation analysis.

373 (3) The deficiency of gauge-based gridded data is mainly attributed to the spatial coverage of  
374 rainfall stations, causing uncertainty to be amplified in extreme precipitation analysis. By correcting



375 these gauge-based gridded data using complementary observations from denser networks of rainfall  
376 stations, extreme precipitation representation may be greatly improved.

377

378 *Data availability.* The co-authors used publicly available data from the Asian Precipitation Highly  
379 Resolved Observational Data Integration Towards Evaluation of Water Resources and the National  
380 Centers for Environmental Information. In addition, rainfall observations in China were obtained  
381 from the National Meteorological Information Center.

382

383 *Author contributions.* XL and YL conceived the study, XL and XF carried out bias correction and  
384 extreme precipitation analysis, XL drafted the paper, and all co-authors jointly worked on enriching  
385 and developing the draft.

386

387 *Competing interests.* The authors declare that they have no conflict of interest.

388

389 *Acknowledgements.* This study was supported by the National Natural Science Foundation of China  
390 (41661144044, 41601026), the National Key R&D Program of China (2016YFA0601601), and the  
391 Science and Technology Planning Project of Yunnan Province, China (2017FB073).

392

### 393 **References**

394 Alexander, L. V.: Global observed long-term changes in temperature and precipitation extremes: A  
395 review of progress and limitations in IPCC assessments and beyond, *Weather & Climate Extremes*,  
396 11, 4–16, <https://doi.org/10.1016/j.wace.2015.10.007>, 2016.



- 397 Andermann, C., Bonnet, S., and Gloaguen, R.: Evaluation of precipitation data sets along the  
398 Himalayan front, *Geochemistry, Geophysics, Geosystems*, 12, Q07023,  
399 <https://doi.org/10.1029/2011gc003513>, 2011.
- 400 Bookhagen, B., Burbank, and D. W.: Toward a complete Himalayan hydrological budget:  
401 Spatiotemporal distribution of snowmelt and rainfall and their impact on river discharge, *Journal of*  
402 *Geophysical Research*, 115, F03019, <https://doi.org/doi:10.1029/2009JF001426>, 2010.
- 403 Chaudhary S., Dhanya C. T., and Vinnarasi R.: Dry and wet spell variability during monsoon in  
404 gauge-based gridded daily precipitation datasets over India, *Journal of Hydrology*, 546, 204–218,  
405 <https://doi.org/10.1016/j.jhydrol.2017.01.023>, 2017.
- 406 Dhar, O. N. and Nandargi, S.: A study of floods in the Brahmaputra Basin in India, *International*  
407 *Journal of Climatology*, 20, 771–781, 2000.
- 408 Dimri, A. P., Thayyen, R. J., Kibler, K., Stanton, A., Jain, S. K., Tullos, D., and Singh, V. P.: A review  
409 of atmospheric and land surface processes with emphasis on flood generation in the Southern  
410 Himalayan rivers, *Science of the Total Environment*, 556, 98 – 115,  
411 <http://dx.doi.org/10.1016/j.scitotenv.2016.02.206>, 2016.
- 412 Donat, M.G., Alexander L.V., Yang, H., Durre, I., Vose R., and Caesar J.: Global land-based datasets  
413 for monitoring climatic extremes, *Bulletin of the American Meteorological Society*, 94, 997–1006,  
414 <http://dx.doi.org/10.1175/BAMS-D-12-00109.1>, 2013.
- 415 Duan, Z., Liu, J., Tuo, Y., Chiogna, G., and Disse, M.: Evaluation of eight high spatial resolution  
416 gridded precipitation products in Adige Basin (Italy) at multiple temporal and spatial scales, *Science*  
417 *of the Total Environment*, 573, 1536–1553, <https://doi.org/10.1016/j.scitotenv.2016.08.213>, 2016.
- 418 Easterling, D. R.: Climate extremes: observations, modeling, and impacts, *Science*, 289, 2068–2074,



- 419 <https://doi.org/doi:10.1126/science.289.5487.2068>, 2000.
- 420 Gain, A. K., Immerzeel, W. W., Sperna Weiland, F. C., and Bierkens, M. F. P.: Impact of climate  
421 change on the stream flow of the lower Brahmaputra: trends in high and low flows based on  
422 discharge-weighted ensemble modelling, *Hydrology and Earth System Sciences*, 15, 1537–1545,  
423 <https://doi.org/10.5194/hess-15-1537-2011>, 2011.
- 424 Guan, Z. H., Chen, C. Y., Ou, Y. X., Fan Y. Q., Zhang Y. S., Chen, Z. M., Bao, S. H., Zu, Y. T., He  
425 X. W., and Zhang M. T. (Eds.): *Rivers and Lakes in Tibet*, Science Press, Beijing, China, pp. 35–39,  
426 1984.
- 427 He, Z., Hu, H., Tian F., Ni G., and Hu Q.: Correcting the TRMM rainfall product for hydrological  
428 modelling in sparsely-gauged mountainous basins, *Hydrological Sciences Journal*, 62, 306–318,  
429 <https://doi.org/10.1080/02626667.2016.1222532>, 2017.
- 430 Immerzeel, W.: Historical trends and future predictions of climate variability in the Brahmaputra  
431 basin, *International Journal of Climatology*, 28, 243–254, <https://doi.org/10.1002/joc.1528>, 2008.
- 432 Immerzeel, W. W., van Beek, L. P. H., and Bierkens, M. F. P.: Climate change will affect the Asian  
433 water towers, *Science*, 328, 1382–1385, <https://doi.org/10.1126/science.1183188>, 2010.
- 434 Janes, T., Mcgrath, F., Macadam, I., and Jones, R.: High-resolution climate projections for south  
435 Asia to inform climate impacts and adaptation studies in the Ganges-Brahmaputra-Meghna and  
436 Mahanadi deltas, *Science of The Total Environment*, 650, 1499 – 1520,  
437 <https://doi.org/10.1016/j.scitotenv.2018.08.376>, 2019.
- 438 Kamal-Heikman, S., Derry, L. A., Stedinger, J. R., and Duncan, C. C.: A simple predictive tool for  
439 lower Brahmaputra River Basin monsoon flooding, *Earth Interactions*, 11, 1 – 11,  
440 <https://doi.org/10.1175/EI226.1>, 2007.



- 441 Khandu, Awange, J. L., Kuhn, M., Anyah, R., and Forootan, E.: Changes and variability of  
442 precipitation and temperature in the Ganges-Brahmaputra-Meghna River Basin based on global  
443 high-resolution reanalyses, *International Journal of Climatology*, 37, 2141–2159,  
444 <https://doi.org/10.1002/joc.4842>, 2017.
- 445 Lakshmi, V., Fayne, J., and Bolten, J.: A comparative study of available water in the major river  
446 basins of the world, *Journal of Hydrology*, 567, 510 – 532,  
447 <https://doi.org/10.1016/j.jhydrol.2018.10.038>, 2018.
- 448 Leander, R. and Buishand, T. A.: Resampling of regional climate model output for the simulation of  
449 extreme river flows, *Journal of Hydrology*, 332, 487 – 496,  
450 <https://doi.org/10.1016/j.jhydrol.2006.08.006>, 2007.
- 451 Lenderink, G., Buishand, A., and van Deursen, W.: Estimates of future discharges of the river Rhine  
452 using two scenario methodologies: direct versus delta approach, *Hydrology and Earth System  
453 Sciences*, 11, 1145–1159, <https://doi.org/10.5194/hess-11-1145-2007>, 2007.
- 454 Liu, Z., Wang, R., and Yao, Z.: Climate change and its impact on water availability of large  
455 international rivers over the mainland Southeast Asia, *Hydrological Processes*, 32, 3966–3977,  
456 <https://doi.org/10.1002/hyp.13304>, 2018.
- 457 Luo, X., Wu, W., He, D., Li, Y., and Ji, X.: Hydrological simulation using TRMM and CHIRPS  
458 precipitation estimates in the lower Lancang-Mekong River Basin, *Chinese Geographical Science*,  
459 29, 13–25, <https://doi.org/10.1007/s11769-019-1014-6>, 2019.
- 460 Malik, N., Bookhagen, B., and Mucha, P. J.: Spatiotemporal patterns and trends of Indian monsoonal  
461 rainfall extremes, *Geophysical Research Letters*, 43, 1710,  
462 <https://doi.org/doi:10.1002/2016GL067841>, 2016.



463 Nishat, B. and Rahman, S. M. M.: Water resources modeling of the Ganges-Brahmaputra-Meghna  
464 River Basins using satellite remote sensing data, *Journal of the American Water Resources*  
465 *Association*, 45, 1313–1327, <https://doi.org/10.1111/j.1752-1688.2009.00374.x>, 2009.

466 Pervez, M. S. and Henebry, G. M.: Spatial and seasonal responses of precipitation in the Ganges  
467 and Brahmaputra river basins to ENSO and Indian Ocean dipole modes: implications for flooding  
468 and drought, *Nat. Hazards Earth Syst. Sci.*, 15, 147–162, <https://doi.org/10.5194/nhess-15-147-2015>,  
469 2015.

470 Prakash, S., Mitra, A. K., Momin, I. M., Rajagopal, E. N., Basu, S., Collins, M., Turner, A. G., Rao,  
471 K. A., and Ashok, K.: Seasonal intercomparison of observational rainfall datasets over India during  
472 the southwest monsoon season, *International Journal of Climatology*, 35, 2326–2338,  
473 <https://doi.org/10.1002/joc.4129>, 2015.

474 Prakash, S., Seshadri, A., Srinivasan, J., and Pai, D. S.: A new parameter to assess impact of rain  
475 gauge density on uncertainty in the estimate of monthly rainfall over India, *Journal of*  
476 *Hydrometeorology*, 20, 821–832, <https://doi.org/10.1175/JHM-D-18-0161.1>, 2019.

477 Rana, S., McGregor, J., and Renwick, J.: Precipitation seasonality over the Indian subcontinent: an  
478 evaluation of gauge, reanalyses, and satellite retrievals, *Journal of Hydrometeorology*, 16, 631–651,  
479 <https://doi.org/10.1175/jhm-d-14-0106.1>, 2015.

480 Ray, P. A., Yang, Y. E., Wi, S., Khalil, A., Chatikavanij, V., and Brown, C.: Room for improvement:  
481 Hydroclimatic challenges to poverty-reducing development of the Brahmaputra River basin,  
482 *Environmental Science & Policy*, 54, 64–80, <https://doi.org/10.1016/j.envsci.2015.06.015>, 2015.

483 Schmidli, J., Frei, C., and Vidale, P. L.: Downscaling from GCM precipitation: a benchmark for  
484 dynamical and statistical downscaling methods, *International Journal of Climatology*, 26, 679–689,



- 485 <https://doi.org/10.1002/joc.1287>, 2006.
- 486 Sillmann, J., Kharin, V. V., Zhang, X., Zwiers, F. W., and Bronaugh, D.: Climate extremes indices  
487 in the CMIP5 multimodel ensemble: Part 1. Model evaluation in the present climate, *Journal of*  
488 *Geophysical Research: Atmospheres*, 118, 1716–1733, <https://doi.org/doi:10.1002/jgrd.50203>,  
489 2013.
- 490 Singh, S., Kumar, R., Bhardwaj, A., Sam, L., Shekhar, M., Singh, A., Kumar, R., and Gupta, A.:  
491 Changing climate and glacio-hydrology in Indian Himalayan Region: a review. Wiley  
492 *Interdisciplinary Reviews: Climate Change*, 7, 393–410. <https://doi.org/10.1002/wcc.393>, 2016.
- 493 Singh, V. P., Sharma, N., and Ojha, C. S. P. (Eds.): *The Brahmaputra Basin water resources*, Kluwer  
494 Academic Publishers, Dordrecht, Netherlands, pp. 17–34, 2004.
- 495 Teutschbein, C. and Seibert, J.: Bias correction of regional climate model simulations for  
496 hydrological climate-change impact studies: Review and evaluation of different methods, *Journal*  
497 *of Hydrology*, 456–457, 12–29, <https://doi.org/10.1016/j.jhydrol.2012.05.052>, 2012.
- 498 Wang, C., Ren, X., and Li, Y.: Analysis of extreme precipitation characteristics in low mountain  
499 areas based on three-dimensional copulas—taking Kuandian County as an example, *Theoretical and*  
500 *Applied Climatology*, 128, 169–179, <https://doi.org/10.1007/s00704-015-1692-7>, 2017.
- 501 Xu, R., Hu, H., Tian, F., Li, C., and Khan, M. Y. A.: Projected climate change impacts on future  
502 streamflow of the Yarlung Tsangpo-Brahmaputra River, *Global and Planetary Change*, 175, 144–  
503 159, <https://doi.org/10.1016/j.gloplacha.2019.01.012>, 2019.
- 504 Yatagai, A., Kamiguchi, K., Arakawa, O., Hamada, A., Yasutomi, N., and Kito, A.: APHRODITE:  
505 Constructing a long-term daily gridded precipitation dataset for Asia based on a dense network of  
506 rain gauges, *Bulletin of the American Meteorological Society*, 93, 1401–1415,



- 507 <https://doi.org/10.1175/bams-d-11-00122.1>, 2012.
- 508 Yucel, I. and Onen, A.: Evaluating a mesoscale atmosphere model and a satellite-based algorithm in  
509 estimating extreme rainfall events in northwestern Turkey, *Nat. Hazards Earth Syst. Sci.*, 14, 611–  
510 624, <https://doi.org/10.5194/nhess-14-611-2014>, 2014.
- 511 Zhang Y., Zheng H., Herron N., Liu X., Wang Z., Chiew, F. H. S., and Parajka, J.: A framework  
512 estimating cumulative impact of damming on downstream water availability, *Journal of Hydrology*,  
513 575, 612–627, <https://doi.org/10.1016/j.jhydrol.2019.05.061>, 2019.





514 **Table 1.** Statistical metrics used in the evaluation of original and corrected APHRODITE estimates.

515 **Table 2.** Detailed description of extreme precipitation indices.

516 **Table 3.** Statistical metrics for daily precipitation during JJAS calculated from original and

517 corrected APHRODITE estimates in the Yarlung Tsangpo-Brahmaputra River Basin (YBRB).

518



519 **Table 1.** Statistical metrics used in the evaluation of original and corrected APHRODITE estimates.

Statistical metric	Equation	Optimal value
Pearson correlation coefficient ( $r$ )	$r = \frac{\sum_{i=1}^n (P_{obs,i} - \overline{P_{obs}})(P_{APH,i} - \overline{P_{APH}})}{\sqrt{\sum_{i=1}^n (P_{obs,i} - \overline{P_{obs}})^2} \sqrt{\sum_{i=1}^n (P_{APH,i} - \overline{P_{APH}})^2}}$	1
Percentage bias ( $PB$ )	$PB = \frac{\sum_{i=1}^n (P_{APH,i} - P_{obs,i})}{\sum_{i=1}^n P_{obs,i}} \times 100$	0
Mean error ( $ME$ )	$ME = \frac{\sum_{i=1}^n (P_{APH,i} - P_{obs,i})}{n}$	0
Mean absolute error ( $MAE$ )	$MAE = \frac{\sum_{i=1}^n  P_{APH,i} - P_{obs,i} }{n}$	0
Root mean squared error ( $RMSE$ )	$RMSE = \sqrt{\frac{\sum_{i=1}^n (P_{APH,i} - P_{obs,i})^2}{n}}$	0

520 Notation:  $n$  means the number of samples;  $P_{obs,i}$  and  $P_{APH,i}$  refer to the observations and the APHRODITE estimates,

521 respectively;  $\overline{P_{obs}}$  and  $\overline{P_{APH}}$  are the mean rain gauge precipitation measurement and the mean APHRODITE

522 estimate, respectively.

523



524 **Table 2.** Detailed description of extreme precipitation indices.

Index	Descriptive name	Definition	Unit
CWD	Consecutive wet days	Maximum number of consecutive days with precipitation $\geq 1$ mm	days
R10mm	Number of heavy precipitation days	Count of days when precipitation $\geq 10$ mm during June, July, August, and September (JJAS)	days
R20mm	Number of very heavy precipitation days	Count of days when precipitation $\geq 20$ mm during JJAS	days
Rx1d	Maximum 1-day precipitation amount	Maximum 1-day precipitation	mm
Rx5d	Maximum 5-day precipitation amount	Maximum consecutive 5-day precipitation	mm
SDII	Simple daily intensity index	Total precipitation during JJAS divided by the number of wet days (when precipitation $\geq 1$ mm)	mm/day

525



526 **Table 3.** Statistical metrics for daily precipitation during JJAS calculated from original and  
 527 corrected APHRODITE estimates in the Yarlung Tsangpo-Brahmaputra River Basin (YBRB).

Physiographic zone	Correction method	$r$	$PB$	$ME$	$MAE$	$RMSE$
				(mm)	(mm)	(mm)
TP	Original	0.80	-9.4	-0.3	1.7	3.4
	Linear scaling	0.81	0.0	0.0	1.7	3.3
	Local intensity scaling	0.81	0.0	0.0	1.5	3.3
	Power transformation	0.79	-0.4	0.0	1.6	3.5
	Quantile-quantile mapping	0.80	3.2	0.1	1.6	3.6
HB	Original	0.81	-24.2	-1.6	3.6	15.9
	Linear scaling	0.93	-0.1	0.0	2.9	8.9
	Local intensity scaling	0.92	-0.1	0.0	2.7	8.8
	Power transformation	0.93	0.3	0.0	2.7	8.8
	Quantile-quantile mapping	0.93	11.3	0.7	3.0	10.7
FP	Original	0.81	-11.4	-1.5	8.0	15.5
	Linear scaling	0.83	-0.3	0.0	7.8	14.2
	Local intensity scaling	0.83	-0.3	0.0	7.3	14.1
	Power transformation	0.82	0.4	0.1	7.5	14.9
	Quantile-quantile mapping	0.82	5.7	0.8	7.6	15.1

528



529 **Figure 1.** Locations of rainfall stations in the Yarlung Tsangpo-Brahmaputra River Basin (YBRB).

530 **Figure 2.** Location of Asian Precipitation Highly Resolved Observational Data Integration Towards

531 Evaluation of Water Resources (APHRODITE) grids over the Tibetan plateau (TP), Himalayan belt

532 (HB), and floodplains (FP).

533 **Figure 3.** Spatial distribution of mean maximum 5-day precipitation amount (Rx5d) during June,

534 July, August, and September (JJAS) in the YBRB based on (a) original APHRODITE, as well as (b)

535 linear scaling (LS)-APHRODITE, (c) local intensity scaling (LOCI)-APHRODITE, (d) power

536 transformation (PT)-APHRODITE, and (e) quantile–quantile mapping (QM)-APHRODITE.

537 **Figure 4.** Box-whisker plot for (a) consecutive wet days (CWD), (b) number of heavy precipitation

538 days (R10mm), (c) number of very heavy precipitation days (R20mm), (d) maximum 1-day

539 precipitation amount (Rx1d), (e) Rx5d, and (f) simple daily intensity index (SDII) during JJAS in

540 the three different physiographic zones (TP, HB, and FP) of YBRB derived from original and

541 corrected APHRODITE estimates.

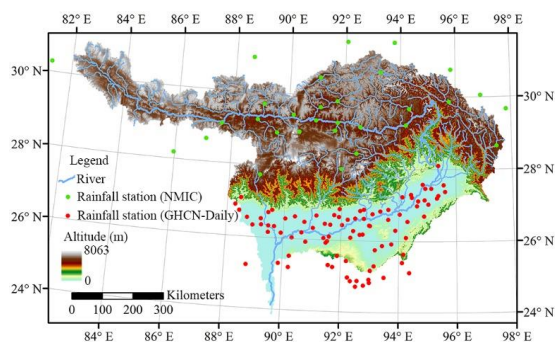
542 **Figure 5.** Relative change rate of (a) CWD, (b) R10mm, (c) R20mm, (d) Rx1d, (e) Rx5d, and (f)

543 SDII during JJAS for the original and corrected APHRODITE estimates.

544 **Figure 6.** Exceedance probabilities of area-averaged Rx5d during JJAS for the original and

545 corrected APHRODITE estimates in the (a) TP, (b) HB, and (c) FP.

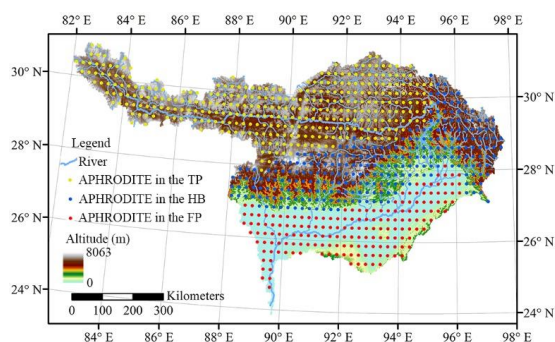
546



547

548 **Figure 1.** Locations of rainfall stations in the Yarlung Tsangpo-Brahmaputra River Basin (YBRB).

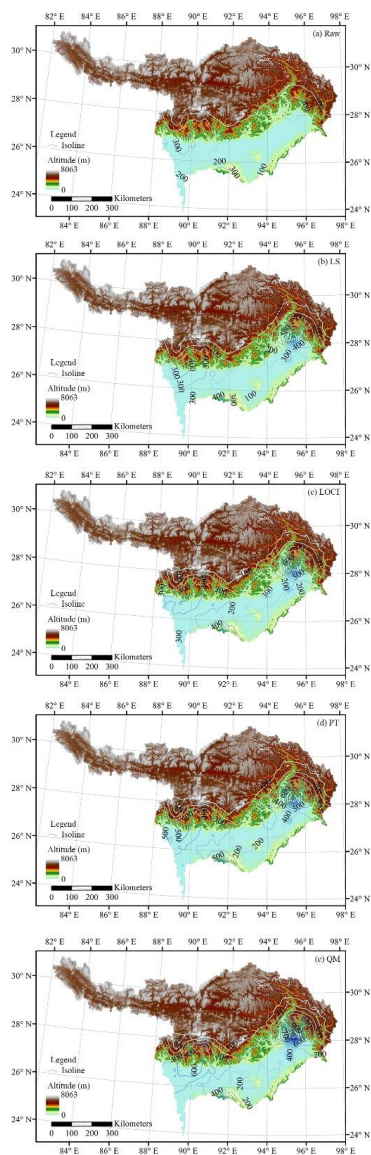
549



550

551 **Figure 2.** Location of Asian Precipitation Highly Resolved Observational Data Integration Towards  
552 Evaluation of Water Resources (APHRODITE) grids over the Tibetan plateau (TP), Himalayan belt  
553 (HB), and floodplains (FP).

554



555

556 **Figure 3.** Spatial distribution of mean maximum 5-day precipitation amount (Rx5d) during June,

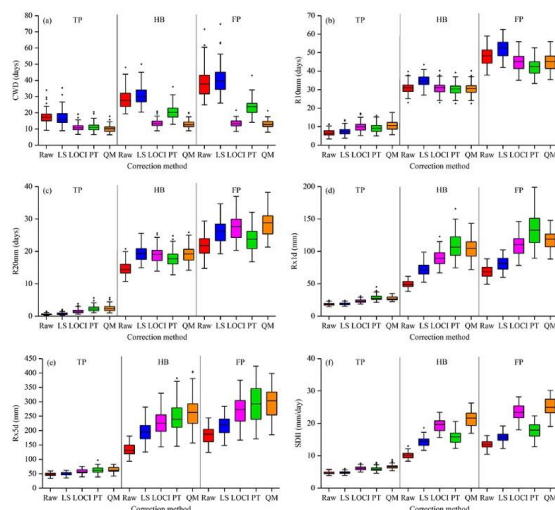
557 July, August, and September (JJAS) in the YBRB based on (a) original APHRODITE, as well as (b)

558 linear scaling (LS)-APHRODITE, (c) local intensity scaling (LOCI)-APHRODITE, (d) power

559 transformation (PT)-APHRODITE, and (e) quantile–quantile mapping (QM)-APHRODITE.

560

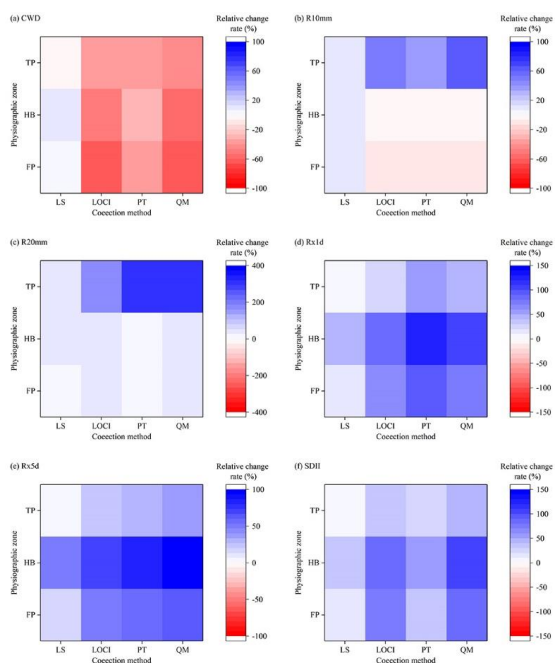




561

562 **Figure 4.** Box-whisker plot for (a) consecutive wet days (CWD), (b) number of heavy precipitation  
563 days (R10mm), (c) number of very heavy precipitation days (R20mm), (d) maximum 1-day  
564 precipitation amount (Rx1d), (e) Rx5d, and (f) simple daily intensity index (SDII) during JJAS in  
565 the three different physiographic zones (TP, HB, and FP) of YBRB derived from original and  
566 corrected APHRODITE estimates.

567

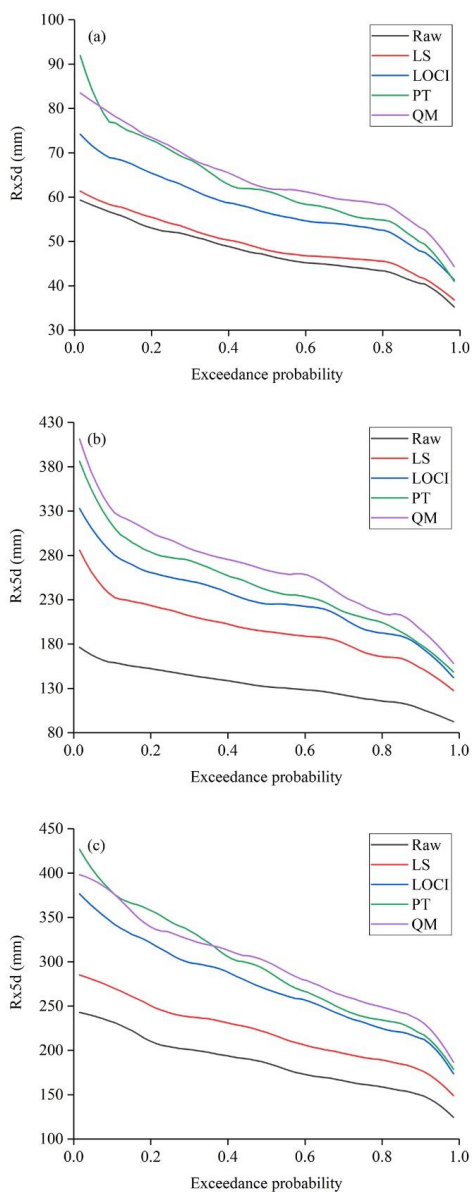


568

569 **Figure 5.** Relative change rate of (a) CWD, (b) R10mm, (c) R20mm, (d) Rx1d, (e) Rx5d, and (f)

570 SDII during JJAS for the original and corrected APHRODITE estimates.

571



572

573 **Figure 6.** Exceedance probabilities of area-averaged Rx5d during JJAS for the original and

574 corrected APHRODITE estimates in the (a) TP, (b) HB, and (c) FP.